Journal of Materials Chemistry A

PAPER

A novel in-situ diffusion strategy to fabricate high performance cathode for low temperature proton-conducting solid oxide fuel cells

Received 00th January 20xx,
Accepted 00th January 20xx

DOI: 10.1039/x0xx00000x

www.rsc.org/

Jie Hou [ab], Lina Miao [a], Jianing Hui [b], Lei Bi [c], Wei Liu [a*], John T. S. Irvine [b*]

Developing new low-cost high-performance cobalt-free cathode materials for low temperature proton-conducting solid oxide fuel cells (H-SOFC) has been an imperative topic. In response to this challenge, we herein develop a novel in-situ Pr diffusion strategy based on $Sm_{0.2}Ce_{0.8}O_{2-\delta}$-$Pr(Pr_{0.5}Ba_{1.5})Cu_3O_{7-\delta}$ (SDC-PBCu, 3:7 wt.%) compound, to achieve a perovskite-related proton-blocking composite cathode (PBCC) $Ce_{1-x}Pr_xO_{2-\delta}$-$Ba_2CeCu_3O_{7.4}$-$Sm_2Ba_{1.33}Ce_{0.67}Cu_3O_9$-CuO (PDC-BCC-SBCC-CuO) for $BaZr_{0.1}Ce_{0.7}Y_{0.2}O_{3-\delta}$-based H-SOFC. The single cell achieves a remarkable performance with the maximum power density (MPD) of 1000 and 566 mW cm^{-2}, corresponding to the interfacial polarization resistance (R_P) of 0.037 and 0.188 Ω cm^2 at 700 and 600 °C, respectively. The XRD results demonstrate that the PBCu phase disappear after the calcination of the mixed SDC-PBCu composite powder at 900 °C, with the formation of four new phases including fluorite structured PDC, orthorhombic layered material BCC, tetragonal perovskite-related SBCC and a small quantity of metallic oxide CuO, being favorable for a superior cathode performance. The ascendant electrochemical performance including the very high MPD and the lower R_P obtained here indicate that the quaternary cobalt-free PBCC PDC-BCC-SBCC-CuO is a preferable alternative for high-performance low-temperature H-SOFC.

1. Introduction

In the present solid oxide fuel cell (SOFC) research, lowering the SOFC operating temperature to low temperatures (LTs, ≤ 600 °C) accompanied with an advisable cell performance is the primary target [1-3]. In virtue of the low activation energy (E_a) and good ionic conductivity, proton-conducting oxides have intriguing potential for high performance low temperature SOFC (HPLT-SOFC) [4-6]. In spite of $BaCeO_3$-based protonic conductors have shown relatively high proton conductivity (10^{-2} S cm^{-1} at 600 °C [7]), its reaction with CO_2 and H_2O hinder the practical application [8-10]. To increase the chemical stability of $BaCeO_3$, one common approach is to partially replace Ce by Zr, and a good component $BaZr_{0.1}Ce_{0.7}Y_{0.2}O_{3-\delta}$ (BZCY) exhibiting both sufficient chemical stability and adequate proton conductivity, has been one of the most popular protonic conductors [11-14].

For proton-conducting SOFC (H-SOFC), as a result of the relatively large E_a of oxygen reduction reaction (ORR), the cathode polarization dominates the cell loss when the temperature is reduced [15]. A good cathode should possess adequate electrical conductivity, good catalytic activity, fine chemical compatibility and a compatible expansion coefficient (TEC) with the electrolyte [16, 17]. By now, the transfer mode in H-SOFC cathode can be divided into four types. The first type, shown in Fig. 1(a), is a single electronic conductor which can only transport electronic defects. Less attention was paid to this type of cathode because the extremely weak ability to transport oxygen ions (O^{2-}) impedes the ORR. Xie et al [18] used $Nd_{0.7}Sr_{0.3}MnO_{3-\delta}$ for $BaCe_{0.4}Zr_{0.3}Sn_{0.1}Y_{0.2}O_{3-\delta}$-based H-SOFC and achieved a poor polarization performance (0.33 Ω cm^2 at 700 °C). Hou et al. [19] also employed $LaNi_{0.6}Fe_{0.4}O_{3-\delta}$ (LNF) cathode for BZCY-based cell and proved it that the electrochemical performance could be greatly improved when compounded with an oxygen ionic conductor $La_2NiO_{4+\delta}$ (LNO). As shown in Fig. 1(b), for the second type of cathode, the H-SOFC cathode can transport electronic defects and protons (H^+) at the same time. This typological cathode material can choose both single mixed protonic and electronic conductors (MPEC) and composite materials composed of an electronic conductor and protonic conducting phase. More attention was paid to the doping of $BaCeO_3$ or $BaZrO_3$-based materials. For example, based on the BZCY electrolyte, $BaCe_{0.5}Bi_{0.5}O_{3-\delta}$ [20] and $BaCe_{0.5}Fe_{0.5}O_{3-\delta}$ [21] obtained the power output of 321 and 395 mW cm^{-2} at 700 °C , respectively. To increase the catalytic activity, the Co-doping is taken into account. Duan et al [1] made use of $BaCo_{0.4}Fe_{0.4}Zr_{0.1}Y_{0.1}O_{3-\delta}$ as the cathode for $BaCe_{0.7}Zr_{0.1}Y_{0.1}Yb_{0.1}O_{3-\delta}$ electrolyte and achieved predominant cell performance. As most single-phase cathode of this type has

[a] CAS Key Laboratory of Materials for Energy Conversion & Collaborative Innovation Center of Suzhou Nano Science and Technology, University of Science and Technology of China, Hefei 230026, PR China. Eamil: wliu@ustc.edu.cn
[b] School of Chemistry, University of St Andrews, KY16 9ST, UK. Eamil: jtsi@st-andrews.ac.uk
[c] Institute of Materials for Energy and Environment, College of Materials Science and Engineering, Qingdao University, Qingdao 266071, PR China.

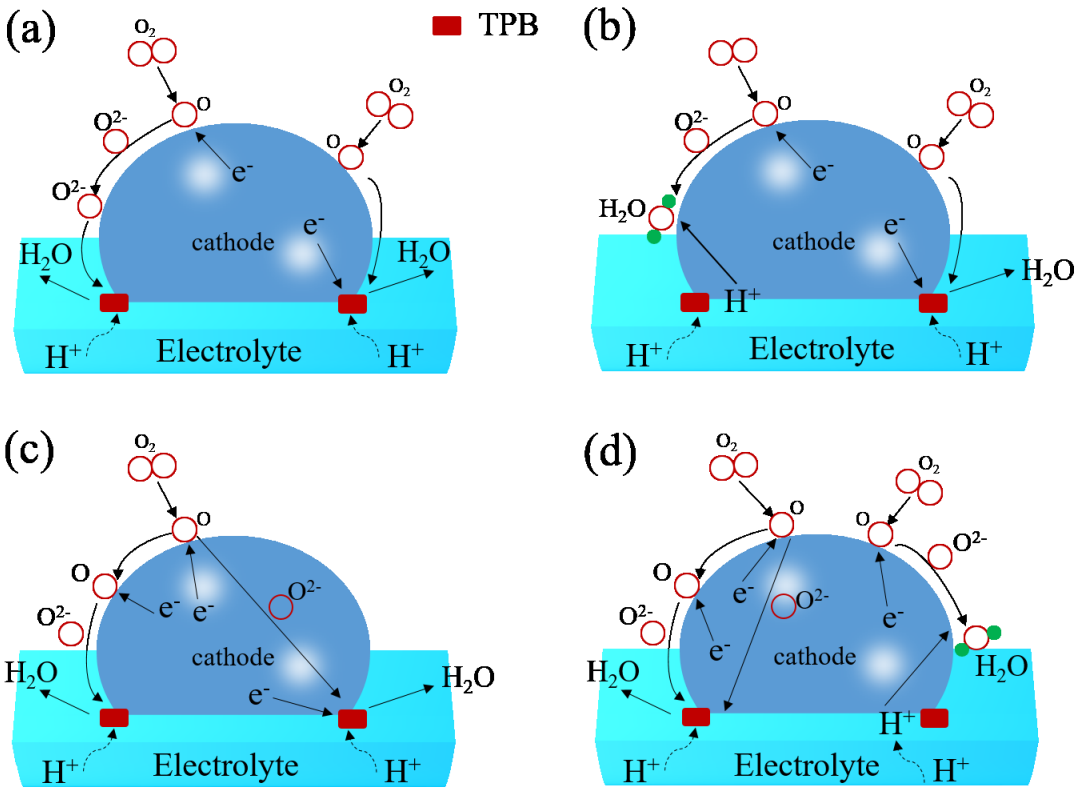

Fig. 1 The transfer mode in H-SOFC cathode.

a relative poor electro-catalytic ability, Zhu et al [22] designed a composite cathode which was made up of BZCY and LNF and achieved superior electrochemical performance with BZCY electrolyte cell. As shown in Fig. 1(c), H-SOFC cathode with the third typological transfer mode can synchronously transport electronic defects and oxygen vacancies, which can also use single mixed ionic and electronic conductors (MIEC), or composite components containing electronic conducting phase and oxygen-ion conductor. The normally used MIEC materials are perovskite, layer-structured perovskite and Ruddlesden-Popper phase, e.g. $La_{0.6}Sr_{0.4}CoO_{3-\delta}$ [23], $SmBaCuCoO_{5+\delta}$ [24], $YBaCuCoO_{5+x}$ [25] and $Pr_{2-x}Sr_xNiO_{4+\delta}$ [26]. Most research was focused on the composite cathode for the superior electrochemical performance with both high electro-catalytic activity and admirable oxygen transfer ability, e.g. $Sm_{0.5}Sr_{0.5}Co_{3-\delta}$-SDC [27] and $Ba_{0.5}Sr_{0.5}FeO_{3-\delta}$-SDC [28]. Differently, the H-SOFC cathode with the forth typological transfer mode allows simultaneous transport oxygen vacancies, electronic defects and protons, which is shown in Fig. 1(d). This kind of materials mostly employ MIEC compounded of protonic conducting phase, e.g. $Sm_{0.5}Sr_{0.5}CoO_{3-\delta}$-$BaCe_{0.8}Sm_{0.2}O_{3-\delta}$ [29], $PrBaCo_2O_{5+\delta}$-BZCY [30], $GaBaCoFeO_{5+\delta}$-BZCY [31] and $La0.6Sr_{0.4}Co_{0.2}Fe_{0.8}O_{3-\delta}$-$BaZr_{0.1}Ce_{0.7}Y_{0.1}Yb_{0.1}O_{3-\delta}$ [32].

In general, the H-SOFC cathode can be divided into two categories. One category is the proton-blocking cathode (PBC, containing the first and third typological transfer mode) and another category is the proton-conducting cathode (PCC, including the second and forth typological transfer mode). In the literature, most single-phase cathode materials have weaker transportation ability of oxygen ions for PBC and lower electronic conductivity for PCC than dual-phase composite cathodes. Both the inferior oxygen ion transfer for PBC and the weak electro-catalytic activity for PCC limit the research of the single-phase cathode materials. For H-SOFC composite cathodes, Sun et al [12] have also found it that the PBC $La_{0.7}Sr_{0.3}FeO_{3-\delta}$-SDC (LSF-SDC) revealed higher electro-catalytic ability than PCC LSF-BZCY, which is correlative with water produced at the cathode, occupying the electrochemical reaction sites and lessening the oxygen partial pressure.

In the light of the problems cobalt-containing H-SOFC cathode faced, e.g. high thermal expansion coefficients (TEC), easy reduction, evaporation and the high cost of cobalt element [19], in this assignment, a novel in-situ Pr diffusion strategy to obtain a cobalt-free quaternary PBCC $Ce_{1-x}Pr_xO_{2-\delta}$-$Ba_2CeCu_3O_{7.4}$-$Sm_2Ba_{1.33}Ce_{0.67}Cu_3O_9$-CuO (PDC-BCC-SBCC-CuO) for BZCY-based H-SOFC is developed. In virtue of the sky-high Pr diffusion activity into SDC [33], SDC and the tetragonal layered perovskite cathode material $Pr(Pr_{0.5}Ba_{1.5})Cu_3O_{7-\delta}$ (PBCu) were selected as the raw materials for the obtainment of the quaternary PBCC. The PDC-BCC-SBCC-CuO might have high electrical conductivity and oxygen kinetics for A-site ordered BCC and SBCC layered structure support mixed-valence transition metal cations ($Cu^{3+}/Cu^{2+}/Cu^{+}$), being capable of providing high electrical conductivity and

maintaining a large oxygen vacancy content, contributing to fast oxygen ion diffusion [34, 35]. Moreover, the high oxygen ionic conductor PDC and electronical conductor CuO are also helpful for achieving high cathode performance. When coupling SDC with PBCu to form a compound as cathode, it is supposed to have a better cell performance.

2. Experimental

2.1. Preparation of powders

PBCu, SDC and BZCY powders were synthesized via a citric acid-nitrate gel combustion process [27, 36]. The raw materials for synthesis of PBCu powders were Pr_6O_{11}, $BaCO_3$, $Cu(NO_3)_2{\bullet}3H_2O$, and Sm_2O_3, $Ce(NO_3)_3{\bullet}6H_2O$ were used for synthesizing SDC. $BaCO_3$, $Zr(NO_3)_4{\bullet}5H_2O$, $Ce(NO_3)_3{\bullet}6H_2O$, $Y(NO_3)_3{\bullet}6H_2O$ served as the crude materials for BZCY powders. After combustion, the as-prepared ash-like powders were calcined at 900, 600 and 1000 °C for 3 h in air to obtain PBCu, SDC and BZCY powders, respectively.

2.2. Fabrication of anode-supported single cells

The NiO-BZCY composite powder with a weight ratio of 65:35 for the anode substrate and anode functional layer (AFL) were prepared by the one-step gel combustion process [27, 36]. The composite powders were calcined at 1000 °C for 3 h and then 20 wt.% starch was added as pore-creating materials to form sufficient porosity in the anode. The anode supported half cells with a tri-layered structure containing anode, AFL (NiO-BZCY composite powders with no starch) and BZCY electrolyte layer, were fabricated by a co-pressing method [37] and then co-fired at 1400 °C for 5 h.

SDC mixed with PBCu in the weight ratio 3:7 thoroughly together with a 10 wt.% ethylcellulose-terpineol binder was used to prepare SDC-PBCu cathode ink. The ink was then painted onto the dense BZCY electrolyte membrane and fired at 900 °C for 3 h in air to form a porous cathode layer. Ag paste and wire were applied to the cathode as a current collector and the conducting wire, respectively. The effective area of the cathode was 0.237 cm^2.

2.3. Characterization and electrochemical measurements

The single cell was tested in a home-made cell testing system at the temperature range of 450-700 °C. Humidified hydrogen (~3%H_2O) at a flow rate of 30 ml min^{-1} and ambient air were used as the fuel and oxidant, respectively. The water vapor pressure about 0.03 atm was achieved by bubbling H_2 through water at about 25 °C. I-V curves of the cells were collected with a DC Electronic Load (ITech Electronics model IT8511) based on a two-probe configuration. The electrochemical impedance spectra were measured under open circuit conditions using an impedance analyzer (CHI604E, Shanghai Chenhua) (0.1-100 kHz, 5 mV as AC amplitude). Ohmic resistance and polarization resistance of the cells under open circuit conditions were determined from the impedance spectra. Phase compositions of SDC-PBCu mixed powders fired at 900 and 950 °C were identified by X-ray powder diffraction on a PANalytical Empyrean Reflection Diffractometer using CuKα1 radiation, and phase structure of the cobalt-free quaternary PBCC PDC-BCC-SBCC-CuO derived from SDC-PBCu was characterized by high-resolution transmission electron microscope (HRTEM, JEM-2010). The microstructures of the cell components were investigated by a scanning electron microscopy (SEM, JEOL JSM-6700F).

3. Results and discussion

3.1. Phase structure and Pr diffusion

As shown in Fig. 2, rietveld analysis of X-ray powder diffraction data reveals that PBCu calcined at 900 °C exhibits a tetragonal layered perovskite structure with P4/mmm space group symmetry and the lattice constant of a=b=3.8918 Å and c=11.6360 Å. The tick marks below the patterns represent the Bragg positions. The lower blue line represents the difference between the observed and calculated intensities. The quality of the agreement between observed and calculated profiles is estimated by profile factor (R_{pf}), weighted profile factor (R_{wp}), expected weighted profile factor (R_{exp}), and reduced chi-square (χ^2). The rietveld refinement converges in a good χ^2 (=2.41) and the reliable parameters guarantee the reliability of refinements.

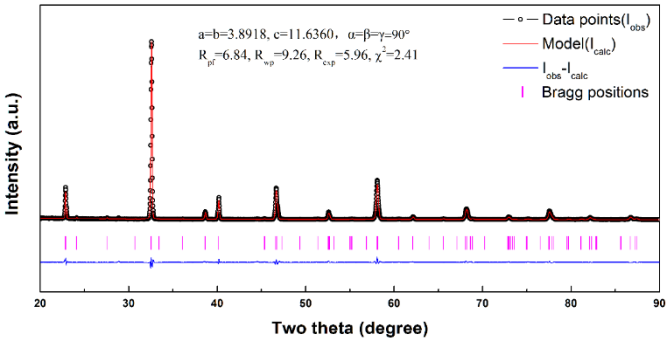

Fig. 2 Rietveld refinement plot of PBCu powders using X-ray powder diffraction data

As is known, in the normal cubic-type perovskite (ABO_3) (shown in Fig. 3(a)), the B-site transition metal cations unite the oxygen ions to form an oxygen 6-fold coordinated scaffold (BO_6), where the alkaline earth or lanthanides ions (A) are located on the vertices of the cube containing the octahedral. The A-site ions tend to have 12-coordination with oxygen to form a stable structure. Nevertheless, in the PBCu structure (shown in Fig. 3(b)), the Pr^{3+} only has 8-coordination with oxygen, which will result in the oxygen deficiency of PrO layer. In this condition, there will be existing a large number of oxygen vacancies in the PrO layer, and thus improve the oxygen ionic conductivity. In addition, the Ba^{2+} has 12-coordination with oxygen and the Ba(Pr)O layer keeps relatively stable. The smaller ionic radius of Pr^{3+} (1.126 Å, 8-coordination with oxygen) than Ba^{2+} (1.61 Å, 12-coordination with oxygen) induces a cationic ordering in alternating layers for layered

perovskites. Then the PBCu could be understood as the single PrO layer alternates with two element

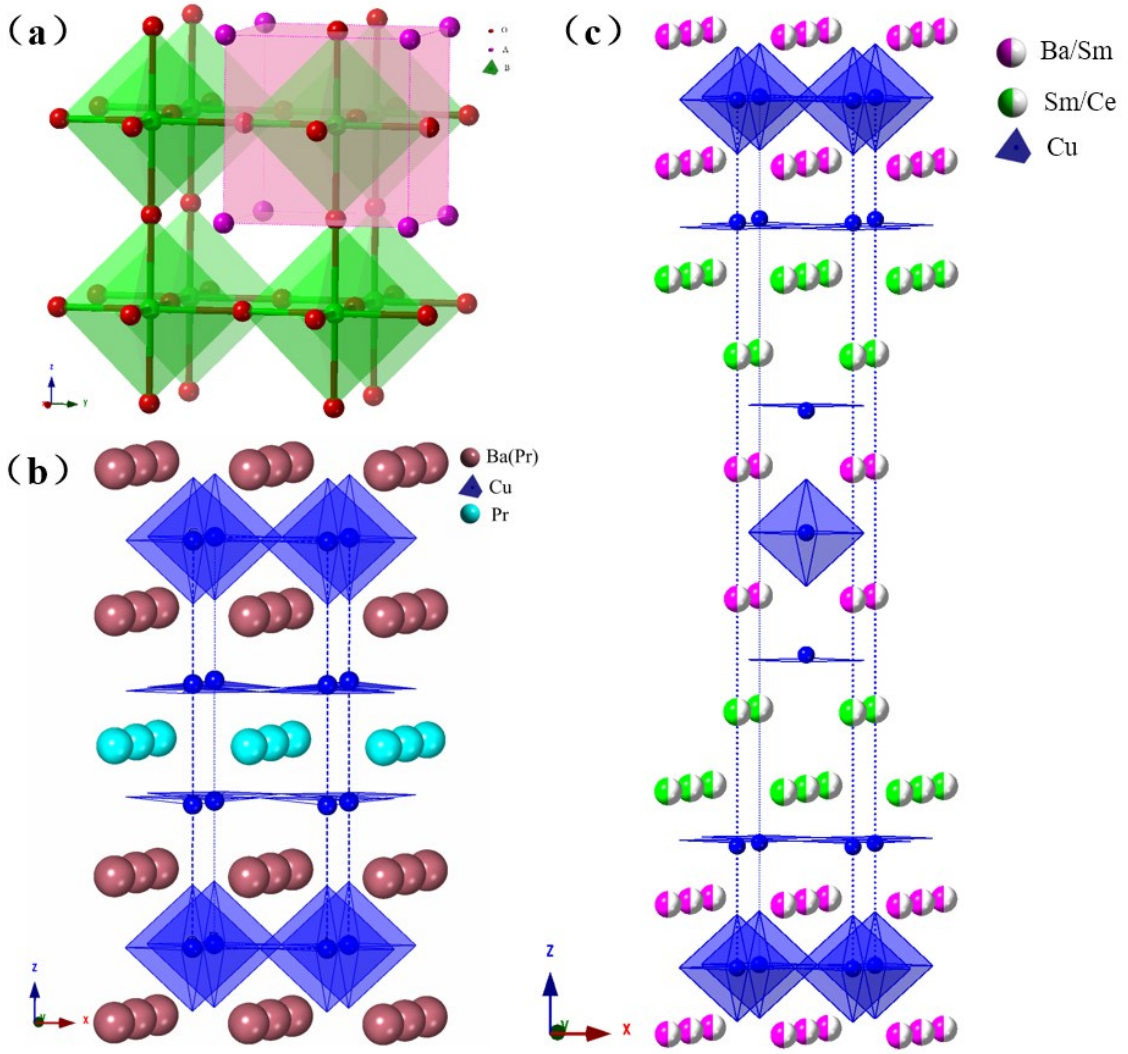

Fig. 3 Structure of (a) normal perovskite (ABO_3), (b) tetragonal PBCu and (c) layerd $Sm_2Ba_{1.33}Ce_{0.67}Cu_3O_9$.

randomly distributed Ba(Pr)O layers, such as $Ba(Pr)O\text{-}CuO_2\text{-}Ba(Pr)O\text{-}Cu'O_2\text{-}PrO\text{-}Cu'O_2$, which can be written as $Pr(Pr_{0.5}Ba_{1.5})Cu_3O_{7-\delta}$ or $Pr(Pr_{0.25}Ba_{0.75})_2Cu_3O_{7-\delta}$. The randomly distributed Pr in the Pr(Ba)O layers could also promote to form the oxygen vacancy defects, which will complement with the large numbers of oxygen vacancy defects in the PrO layers to transfer oxygen ions efficiently in two different dimensional layers. The Pr-O bond is shorter than Ba-O bond, leading to a different chemical force of the PrO layer and Ba(Pr)O layer with CuO_6 octahedral, which will compress the PrO layer with the stretch of the Ba(Pr)O layer, resulting in the formation of the tetragonal layered structure [15, 38]. Notedly, in virtue of the oxygen deficiency in the PrO layer, the near Cu only has an oxygen 5-fold coordinated scaffold (BO_5).

The phases of SDC-PBCu mixed powders calcined at 900, 950 °C for 3 h and 700 °C for 20 h after the treatment at 900 °C were studied by the powder XRD technique which is shown in Fig. 4(a). Indexing of these patterns reveals that SDC has a fluorite structure with cubic symmetry of space group $Pm\bar{3}m$ and PBCu possesses the layered tetragonal structure showed in Fig. 2 and Fig. 3. Interestingly, apart from typical peaks corresponding to SDC could be found in the SDC-PBCu pattern, numerous reflection peaks corresponding to PBCu disappear and some new second-phase reaction peaks appear, indicating that obvious reaction occur between the SDC and PBCu phases and the PBCu phase structure has been changed. Seen from Fig. 4(a), when the calcination temperature of mixed SDC-PBCu powders raised from 900 °C to 950 °C, no further reactions can be observed, which illustrates that the reaction has no expansion and the new second-phase resultants are steady. It can also be observed that almost no growth of the secondary phases after the treatment of SDC-PBCu composite at 700 °C for 20 h, suggesting the reaction between SDC and PBCu mainly happened at the cathode firing temperature (900 °C) and such reaction was kinetically steady at fuel cell testing temperatures (such as 700 °C). Moreover, the SDC-PBCu has no phase reaction with BZCY when compounded SDC-PBCu (after treatment at 900 °C) with BZCY and annealed at 900 °C for 10

h (Supplementary Fig. S1), illustrating the superior chemical compatibility between SDC-PBCu composite and BZCY electrolyte. The phenomenon that the PBCu phase has been changed is related to the report that Pr element easily migrated into SDC phase to substitute Sm and Ce element, forming $Ce_{1-x}Pr_xO_{2-\delta}$ [33]. Chiba et al [33] have found that the material $Ce_{1-x}Pr_xO_{2-\delta}$ can maintain the cubic fluorite structure when the Pr content is below 0.9 and the $PrO_{2-\delta}$ can dissolve in CeO_2 illimitably to form a solid solution. When the Pr content in $Ce_{1-x}Pr_xO_{2-\delta}$ raises from 0 to 0.9, the conductivity and the oxygen vacancy concentration increase evidently, which might make it clear that the Pr element could react with CeO_2 facilely. The substitution of Pr for Sm and Ce elements will result in the Sm and Ce cations transporting to the Pr-sites in the PBCu structure (containing the PrO layer and the Ba(Pr)O layers) and creating new layered structured materials.

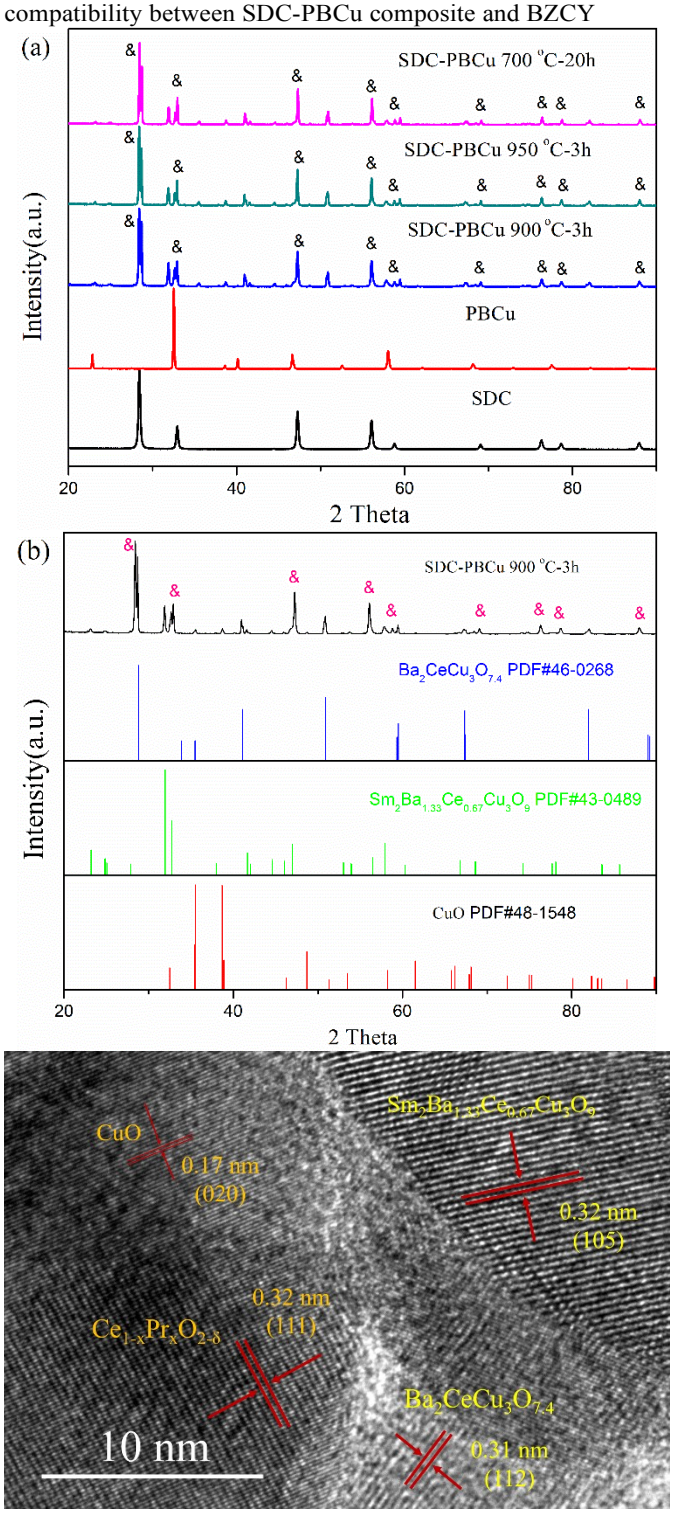

Fig. 4(a) XRD patterns of SDC, PBCu fired at 600, 900 °C for 3 h and the dry-mixed composite powder SDC-PBCu fired at 900, 950 °C for 3h, and 700 °C for 20 h after annealing at 900 °C, respectively; (b) The comparison of XRD patterns of SDC-PBCu and $Ba_2CeCu_3O_{7.4}$ (PDF 46-0268), $Sm_2Ba_{1.33}Ce_{0.67}Cu_3O_9$ (PDF 43-0489) and CuO (PDF 48-1548); (c) High-resolution TEM (HRTEM) image of the quaternary PBCC PDC-BCC-SBCC-CuO derived from SDC-PBCu annealed at 900 °C. The symbol & represents the typical peaks of cubic phase $Ce_{1-x}Pr_xO_{2-\delta}$.

The SDC-PBCu composite powder calcined at 900 °C was indexed to find the reactants. The comparison of the XRD patterns of SDC-PBCu and the indexed materials in the powder diffraction files (JCPDS) is plotted in Fig.4(b), from which we can find that the fired SDC-PBCu consists of $Ce_{1-x}Pr_xO_{2-\delta}$, $Ba_2CeCu_3O_{7.4}$, $Sm_2Ba_{1.33}Ce_{0.67}Cu_3O_9$ and a small quantity of CuO. When the element Sm and Ce getting into the PBCu layered structure synchronously, it forms a tetragonal layered structure $Sm_2Ba_{1.33}Ce_{0.67}Cu_3O_9$ (as shown in Fig. 3(c)), in which two continuous Ba(Sm)O layers alternate with two continuous Sm(Ce)O layers. The element ration in the Ba(Sm)O layer is Ba0.665Sm0.335 (element randomly distributed) and the composition is Sm0.665Ce0.335 (element randomly distributed) for the Sm(Ce)O layer. In two continuous Sm(Ce)O layers, the Sm(Ce) only has 8-coordination with oxygen, promoting to produce a lot of oxygen vacancies with oxygen 5-fold coordinated scaffolds (BO_5) nearby, which could provide the pathways for the transportation of oxygen ions efficiently. With the consideration of the mixed-valence of Cu which supports high electronic conductivity, the new phase material $Sm_2Ba_{1.33}Ce_{0.67}Cu_3O_9$ should possess high electro-catalytic ability for ORR at the cathode and high oxygen transfer rate that is beneficial for the cell cathode performance.

As the Pr element can displace the Ce in CeO_2 in massive quantities, most Ce element may enter the lattice of PBCu and a novel layered structure $Ba_2CeCu_3O_{7.4}$ come into being, which has the similar phase structure with PBCu. However, unlike PBCu, the Ce^{3+} has a larger ionic radius (1.143 Å, 8-coordination with oxygen; 1.34 Å, 12-coordination with oxygen) compared with Pr^{3+} (1.126 Å, 8-coordination with oxygen) and the 12-oxygen coordinated structure generate a more stable CeO layer. For the 12-oxygen coordinated Ce^{3+} (1.34 Å) has a closer ionic radius with Ba^{2+} (1.61 Å, 12-coordination with oxygen), by PBCu lattice, the formation of CeO layer can expand the crystal lattice with the BaO layer being compressed, leading to the formation of orthorhombic layered material $Ba_2CeCu_3O_{7.4}$. The irregular phase structure and the mixed-valence of Cu in $Ba_2CeCu_3O_{7.4}$ would boost the generation of the oxygen deficit and the acquirement of high electrical conductivity. Furthermore, CuO is an electronical conductor, with high electro-catalytic activity. Then both CuO and the orthorhombic

layered structured $Ba_2CeCu_3O_7$ are helpful for achieving considerable cathode properties. These reactants are confirmed by the HRTEM result

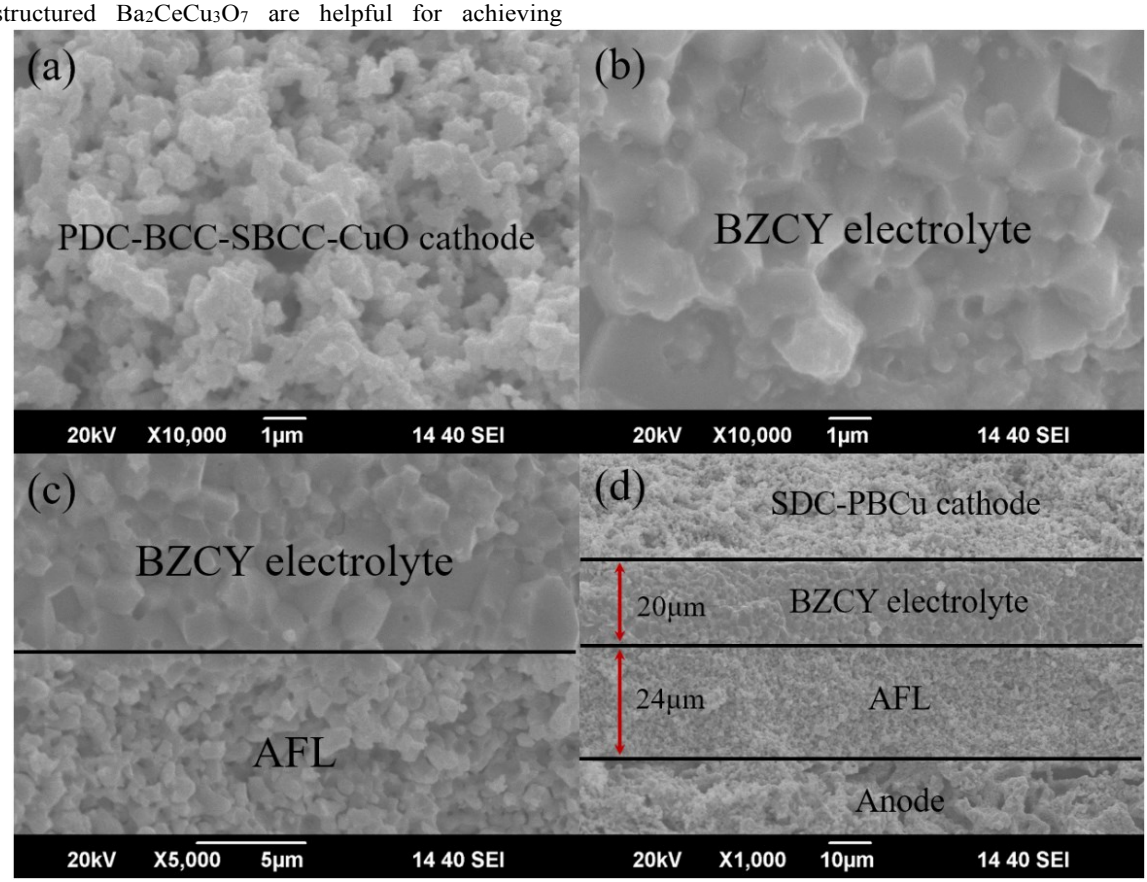

Fig. 5 Cross-section SEM images of (a) PDC-BCC-SBCC-CuO cathode layer, (b) BZCY electrolyte layer, (c) the interface between AFL and BZCY membrane, and (d) the four-layer single cell with an AFL and PDC-BCC-SBCC-CuO cathode after testing.

of SDC-PBCu annealed at 900 °C, as shown in Fig. 4(c). It can be clearly seen that the quaternary PBCC PDC-BCC-SBCC-CuO was formed with the Pr diffusion strategy based on SDC-PBCu compound. The lattice spacings of 0.32, 0.17, 0.32 and 0.31 nm correspond to the (111) crystal plane of $Ce_{1-x}Pr_xO_{2-\delta}$, the (020) crystal plane of CuO, the (105) crystal plane of $Sm_2Ba_{1.33}Ce_{0.67}Cu_3O_9$ and the (112) crystal plane of $Ba_2CeCu_3O_{7.4}$, respectively. Although the SDC-PBCu composite after calcined at 900 °C can not be incapable of retaining the SDC and PBCu phase structure non-destructively, all the new phase structure materials $Ce_{1-x}Pr_xO_{2-\delta}$, $Ba_2CeCu_3O_{7.4}$, $Sm_2Ba_{1.33}Ce_{0.67}Cu_3O_9$ and CuO could advance the occurrence of ORR. The mixed cathode material with both high electro-catalytic and ORR ability might transfer the oxygen ions (O^{2-}) timely, boosting the dissociation of the oxygen molecule and taking the ORR in progress, which is favorable for improving the electrochemical performance. By applying this mixed PBCC material PDC-BCC-SBCC-CuO to H-SOFC, it supposed to have preeminent performance output in principle. Therefore, we decided to evaluate the electrochemical performance on the BZCY electrolyte-based single cell to check it further.

3.2. Microstructures

It can be observed from Fig. 5(a) that the PDC-BCC-SBCC-CuO cathode active layer possesses a uniform and porous structure with the particles interconnecting well with each other, which are almost in nanoscale (400-800 nm) with continuous pores, radically favoring gas diffusion and electrochemical reactions in the cathode. The relatively large particle (~ 800 nm) in the cathode is correlative with the good sintering activity of Cu. However, in the light of high electro-catalytic activity of Cu, the cathode is also expected to have a predominant electrochemical performance as an H-SOFC PBC material. Seen from Fig. 5(b), the BZCY electrolyte is dense with the grain size ranges from around 1 to 2 μm which can prevent the gas leakage and allows the transportation of protons (H^+) efficiently. The BZCY electrolyte membrane bonds tightly with the NiO-BZCY AFL, which can be seen from Fig. 5(c). Although the single cell has suffered a heating and subsequent cooling process during testing, the firm adherence confirms that the BZCY film shows a good thermal matching with the AFL. The particle size in the AFL is around 1 μm, which could provide abundant triple phase boundaries (TPBs) promoting the rapid dissociation of the fuel gas (for example, H_2). Moreover, in the continuous porous AFL, the pore size and the porosity could affect the rate of gas diffusion from the anode to the AFL layer. As the pores in AFL were mainly obtained by the reduction of NiO in NiO-BZCY

AFL layer, an appropriate proportion of NiO could be able to guarantee sufficient porosity and adequate numbers and length of NiO-BZCY-gas TPBs, which is closely related with the whole cell performance. In this work, the NiO-BZCY with 65 wt.% NiO is used as AFL for the BZCY-based cell to evaluate the performance of PDC-BCC-SBCC-CuO cathode. As shown in Fig. 5(d), all the anode, AFL and cathode has a porous structure. The starch has been added to the anode as the pore forming materials, while the pore size in AFL is much smaller than that of the anode. The small pores in AFL provide the electrochemical reaction sites for H_2 dissociation, while the larger pores in anode ensure the fast diffusion of fuel gas. Both the AFL and cathode are well adhered on both sides of dense BZCY membrane and the four layers (including anode, AFL, BZCY electrolyte and SDC-PBCu cathode) in the single cell have no sign of cracking or delamination, indicating the four-layer structured single cell with an AFL could keep the good microstructures and no thermal mismatch happened during the thermal cycles. The thickness of electrolyte is ~ 20 μm and the thickness for AFL is ~ 24 μm. In this study, based on the excellent H-SOFC structure, it is expected to obtain impressive electrochemical performance in low temperatures when the mixed PBCC PDC-BCC-SBCC-CuO is applied as the cathode for BZCY-based cell.

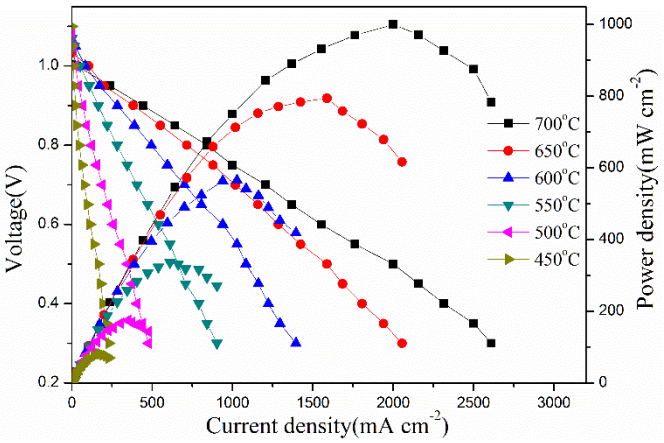

3.3. Electrochemical performance of the single cell

Fig. 6 I-V and I-P curves of the single cell NiO-BZCY|AFL|BZCY|PDC-BCC-SBCC-CuO measured at 450-700 °C.

To evaluate the performance of the mixed PBCC PDC-BCC-SBCC-CuO for H-SOFC in LT operation range, the button cell with an NiO-BZCY anode, an AFL, the BZCY electrolyte and PDC-BCC-SBCC-CuO cathode was fabricated and measured

Table 1 Comparison of the MPD (mW cm^{-2}) performance of cobalt-free composite PBCs using $BaCeO_3$-based cell reported in the literature and in the present study.

Year	Cathode	Electrolyte (Thickness, μm)	700	650	600	550	500	450	Ref
2010	$Ba_{0.5}Sr_{0.5}FeO_{3-\delta}$-SDC	$BaZr_{0.1}Ce_{0.7}Y_{0.2}O_{3-\delta}$ (20)	696	517	315	174	87		28
2011	$Sm_{0.5}Sr_{0.5}Fe_{0.8}Cu_{0.2}O_{3-\delta}$-SDC	$BaZr_{0.1}Ce_{0.7}Y_{0.1}Yb_{0.1}O_{3-\delta}$ (15)	505	398	289	195	121		39
2011	$La_{0.7}Sr_{0.3}FeO_{3-\delta}$-SDC	$BaZr_{0.1}Ce_{0.7}Y_{0.2}O_{3-\delta}$ (15)	449	330	246	167	101		40
2011	$La_{0.7}Sr_{0.3}FeO_{3-\delta}$-SDC	$BaZr_{0.1}Ce_{0.7}Y_{0.2}O_{3-\delta}$ (13)		542	407	265	175	97	41
2012	$Ba_{0.5}Sr_{0.5}Fe_{0.9}Ni_{0.1}O_{3-\delta}$-SDC	$BaZr_{0.1}Ce_{0.7}Y_{0.2}O_{3-\delta}$ (25)	362	323	268	206			42
2014	$La_{0.6}Pr_{0.2}Sr_{0.2}FeO_{3-\delta}$-SDC	$BaZr_{0.1}Ce_{0.7}Y_{0.2}O_{3-\delta}$ (15)	488	416	340	261			43
2014	$La_2NiO_{4+\delta}$-$LaNi_{0.6}Fe_{0.4}O_{3-\delta}$73	$BaZr_{0.1}Ce_{0.7}Y_{0.2}O_{3-\delta}$ (20)	590	469	298	203			19
2015	$Pr_{0.6}Sr_{0.4}Cu_{0.2}Fe_{0.8}O_{3-\delta}$-SDC	$BaZr_{0.3}Ce_{0.5}Y_{0.2}O_{3-\delta}$ (20)	546	469	330	233	178		44
		$BaZr_{0.1}Ce_{0.7}Y_{0.2}O_{3-\delta}$ (-)	712	556	351	219	132		
2015	$La_2NiO_{4+\delta}$-$LaNi_{0.6}Fe_{0.4}O_{3-\delta}$	$BaZr_{0.1}Ce_{0.7}Y_{0.2}O_{3-\delta}$ (14)	708	542	352				6

This work	PDC-BCC-SBCC-CuO	$BaZr_{0.1}Ce_{0.7}Y_{0.2}O_{3-\delta}$ (20)	1000	794	566	336	175	83

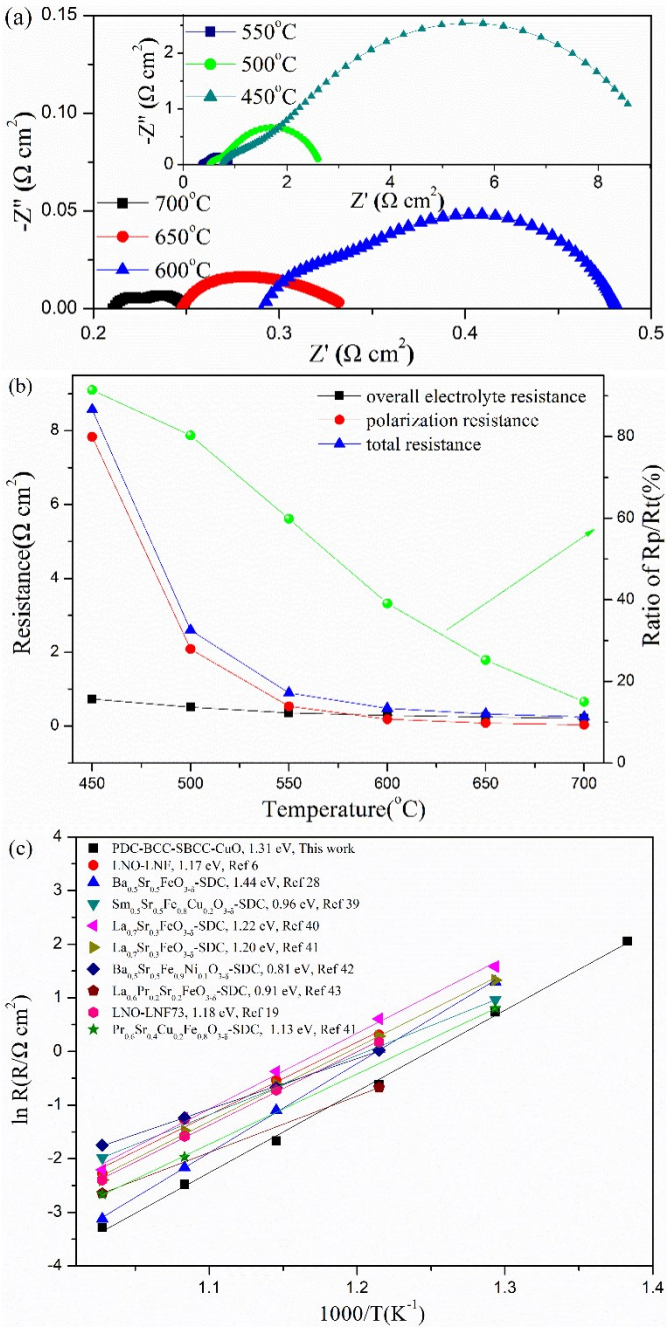

Fig. 7 (a) EIS of the single cell NiO-BZCY|AFL|BZCY|PDC-BCC-SBCC-CuO measured under open-circuit conditions from 450 to 700 °C, (b) the temperature dependence of the ohmic resistance (R_O), polarization resistance (R_P) and total resistance (R_T), as well as the ratio R_P/ R_T of the single cell with PDC-BCC-SBCC-CuO cathode, and (c) the Arrhenius plots for Rp of PDC-BCC-SBCC-CuO estimated from the EIS in this study and the cobalt-free composite PBCs reported in the literature.

under conventional conditions using static air as the oxidant and humidified hydrogen as the fuel gas. Fig. 6 shows typical I-V and I-P curves of the cell NiO-BZCY|AFL|BZCY|PDC-BCC-SBCC-CuO measured at 450-700 °C. The open-circuit voltages (OCVs) of the cell with PDC-BCC-SBCC-CuO cathode after anode reduction are 1.004, 1.033, 1.052, 1.069, 1.083 and 1.1V, accompanied with the corresponding maximum power densities (MPDs) of 1000, 794, 566, 336, 175 and 83 mW cm^{-2} at 700, 650, 600, 550, 500 and 450 °C, respectively. The high OCV values confirm that the electrolyte membrane is sufficiently dense to resist gas leakage. As shown in Table 1, the single cell with PDC-BCC-SBCC-CuO cathode shows higher MPDs than most PBCCs reported in the literature at all testing temperatures. Although LSF-SDC [41] displays a little higher MPD output than PDC-BCC-SBCC-CuO at 450 °C, the cell performance of PDC-BCC-SBCC-CuO cathode based on $BaCeO_3$-based electrolyte shows almost the largest MPDs ever reported at above 500 °C, suggesting the outstanding electrochemical properties of the mixed PBCC PDC-BCC-SBCC-CuO in the LT operation range, which may be attributed to high electro-catalytic activity of BCC and SBCC.

However, in the developed cobalt-free PBCCs, although quite a few PBCCs present preferable cell performance, such as $Ba_{0.5}Sr_{0.5}FeO_{3-\delta}$-SDC [28], $Sm_{0.5}Sr_{0.5}Fe_{0.8}Cu_{0.2}O_{3-\delta}$-SDC [39], $La_{0.6}Pr_{0.2}Sr_{0.2}FeO_{3-\delta}$-SDC [43] and $La_2NiO_{4+\delta}$-$LaNi_{0.6}Fe_{0.4}O_{3-\delta}$ [6, 19], most PBCCs possess better performance only at intermediates (600-800 °C, e.g. 700 °C) while the performance at LT down to 500 °C is inferior. Simultaneously, the PDC-BCC-SBCC-CuO has similar performance output with $La_{0.7}Sr_{0.3}FeO_{3-\delta}$-SDC [41] and $Pr_{0.6}Sr_{0.4}Cu_{0.2}Fe_{0.8}O_{3-\delta}$-SDC [44] at 500 °C and much higher MPD performance than the reported cobalt-free composite PBCs at the temperature range 550-700 °C, which indicates that PDC-BCC-SBCC-CuO is a preferable HPLT cobalt-free PBC material for H-SOFC.

In the EIS plots shown in Fig. 7(a), the high-frequency intercept corresponds to the ohmic resistance (R_O) of the cell, consisting of the resistance of the electrolyte, the resistance of the electrodes and some contact resistance associated with the interfaces of the components. The low-frequency intercept corresponds to the total resistance (R_T) and the difference between the two intercept indicates the interfacial polarization resistance (R_P) of the cell. In order to further validate the resistance values of the cell, the equivalent circuit was used to fit the impedance plots. The equivalent circuit model could be made of a resistance (R) associated in series with two distributed elements, composed by a constant phase element (CPE) in parallel with a resistance. We found that the resistance obtained from the fitting equivalent circuit matched well with the values obtained from the intercepts at 600 °C (Supplementary Fig. S2). All resistances including R_O, R_P and R_T decrease with increasing temperature, which can be seen from Fig. 7(b), stating it clearly that the corresponding electrochemical reaction processes are thermally activated. The R_P of the single cell with PDC-BCC-SBCC-CuO cathode increases from 0.037 to 7.835 Ω cm^2 with the temperature decreasing from 700 to 550 °C. The R_O only

increases from 0.212 to 0.737 Ω cm^2 under the same working conditions. The R_P values are 0.037, 0.084, 0.188, 0.538, 2.087 and 7.835 Ω cm^2, with the corresponding R_O values of 0.212, 0.248, 0.293, 0.361, 0.512 and 0.737 Ω cm^2 at 700, 650, 600, 550, 500 and 450 °C, respectively. Evidently, the ratios of R_P/R_T are 15.02%, 25.27%, 39.11%, 59.88%, 80.30% and 91.41% with the decreasing temperature ranging from 700 to 450 °C, and the R_P controls the downhill trend of R_T below 550°C, playing a leading role in determining the total resistance of the single cell. Then more attention could be paid to the exploration of electrode materials with high activity at low temperatures to decrease the R_P, thus enhancing the performance of BZCY-based cell, and benefiting the SOFC LT operation.

As shown in Fig. 7(c), the E_a of multifarious cobalt-free composite PBCs calculated by the Arrhenius equation is listed. Though the E_a of the R_P is higher than that of most reported cobalt-free PBCCs in the literature, corresponding to the value of 1.31 eV for PDC-BCC-SBCC-CuO, $Ba_{0.5}Sr_{0.5}FeO_{3-\delta}$-SDC [28] has a much higher E_a (1.44 eV). The $La_{0.6}Pr_{0.2}Sr_{0.2}FeO_{3-\delta}$-SDC [43] cathode possesses almost equivalent polarization performance with PDC-BCC-SBCC-CuO cathode in this work at lower operation temperatures, which has the R_P value of 0.51 Ω cm^2 at 550 °C. Worthy of attention is that the R_P of PDC-BCC-SBCC-CuO is lowest in the developed cobalt-free composite PBCs except for the R_P of $La_{0.6}Pr_{0.2}Sr_{0.2}FeO_{3-\delta}$-SDC [43] at 550 °C, indicating the preeminent ORR catalytic activity and excellent oxygen transfer ability, which could make it clear that the PDC-BCC-SBCC-CuO is an outstanding PBC material for H-SOFC. The relatively high E_a of PDC-BCC-SBCC-CuO in the whole operating temperature range could also illustrate it that the cathode has a strong dependency relationship with the testing temperature. Then the R_P of PDC-BCC-SBCC-CuO increases more rapidly, being consist with the little higher cell MPD performance degradation rate which could be seen from Table 1. This phenomenon may be ascribed to the relatively fast decay of electro-catalytic ability for the manifold phases in PDC-BCC-SBCC-CuO cathode, affecting the numbers of the effective TPBs and the ORR kinetics at LTs down to 450 °C. That is to say, the invalid TPBs hinder the ORR kinetics and the oxygen transfer rate.

In addition, the long-term stability performance of the single cell with PDC-BCC-SBCC-CuO cathode was conducted. The OCV kept stable for 60 h which indicates that the structure of the single cell was not broken after operating 60 h under open circuit condition (Supplementary Fig. S3(a)). Interestingly, the power density is around 450 mW cm^{-2} at the beginning of the stability test under 0.7 V at 600 °C, and then increase to about 500 mW cm^{-2} after 25 h. The power output kept stable at 500 mW cm^{-2} for another 20 h and then decrease to 450 mW cm^{-2}. Anyhow, during the 60 h stability test, the single cell power output almost has no degradation (Supplementary Fig. S3(b)). The good long-term performance could illustrate that the PDC-BCC-SBCC-CuO cathode has fine chemical stability against water vapor and CO_2 in ambient air, and the PDC-BCC-SBCC-CuO cathode obtained with Pr diffusion strategy is a promising cathode for HPLT H-SOFCs.

In view of the reaction between SDC and PBCu has some infaust effect to the cell performance at lower temperatures, especially at the temperature down to 450 °C, the ionic conductive phase SDC could be replaced by other structured materials which should have no adverse reaction with PBCu, avoiding both new phase resultant to help using the high oxygen ion conductivity and oxygen catalytic ability to design the low-cost cobalt-free PBC material. The method of doping of A-site or B-site cations in the PBCu layered perovskite structure can also be adopted to obtain a good thermal-matching material, which could be conducive to exert wonderful intrinsic properties of PBCu.

4. Conclusions

The present work develops an in-situ Pr diffusion strategy to achieve a quaternary compound PDC-BCC-SBCC-CuO acting as a PBC candidate for LT H-SOFC. After the treatment of the composite powder SDC-PBCu at 900 °C, several reaction peaks in XRD appeared, which might be attributed to the easily diffusion of Pr element into SDC phase to form fluorite structured solid solution $Ce_{1-x}Pr_xO_{2-\delta}$ with higher oxygen ion conductivity and oxygen vacancy concentration, thus improving the cathode ORR kinetics and the transportation capacity of oxygen. The phenomenon of Pr diffusion may result in the migration of Sm and Ce, occupying the Pr-sites in PBCu layered structure with the formation of several new phase materials containing fluorite structured $Ce_{1-x}Pr_xO_{2-\delta}$, orthorhombic layered material $Ba_2CeCu_3O_{7.4}$, tetragonal perovskite-related $Sm_2Ba_{1.33}Ce_{0.67}Cu_3O_9$ and the metallic oxide CuO. To some extent, the new phase materials could boost the whole ORR at the cathode for the fine oxygen transfer speed and electro-catalytic ability. With the BZCY electrolyte and an NiO-BZCY AFL, the PDC-BCC-SBCC-CuO PBC candidate achieved an encouraging performance with the MPD of 1000, 794, 566, 336, 175 and 83 mW cm^{-2}, and the R_P of 0.037, 0.084, 0.188, 0.538, 2.087 and 7.835 Ω cm^2 at 700, 650, 600, 550, 500 and 450 °C, respectively. The almost highest power output above 500 °C compared with the reported cobalt-free PBCCs on $BaCeO_3$-based H-SOFC in the literature and the nearly lowest polarization properties reveal the commendable potential for working in LTs. Although the E_a of PDC-BCC-SBCC-CuO cathode is slightly higher, the encouraging cell performance at LTs could illustrate it that the novel high catalytic activity cobalt-free PBC PDC-BCC-SBCC-CuO is a superior alternative for HPLT H-SOFC.

Acknowledgements

This work was supported by the National Nature Science Foundation of China (Grant Nos: 21676261, U1632131 and 51602238). The authors acknowledge the financial support of the Royal Society of Edinburgh for a RSE BP Hutton Prize in Energy Innovation and EPSRC Platform grant, EP/K015540/1. We also would like to thank the support from China Scholarship Council (No. 201606340101).

Notes and references

1. C. C. Duan, J. H. Tong, M. Shang, S. Nikodemski, M. Sanders, S. Ricote, A. Almansoori and R. O'Hayre, *Science*, 2015, **349**, 1321-1326.
2. J. Hou, L. Bi, J. Qian, Z. Zhu, J. Zhang and W. Liu, *Journal of Materials Chemistry A*, 2015, **3**, 10219-10224.
3. E. D. Wachsman and K. T. Lee, *Science*, 2011, **334**, 935-939.
4. L. Bi, S. Boulfrad and E. Traversa, *Chemical Society Reviews*, 2014, **43**, 8255-8270.
5. L. Bi, E. H. Da'as and S. P. Shafi, *Electrochemistry Communications*, 2017, **80**, 20-23.
6. J. Hou, J. Qian, L. Bi, Z. Gong, R. Peng and W. Liu, *J. Mater. Chem. A*, 2015, **3**, 2207-2215.
7. G. Ma, T. Shimura and H. Iwahara, *Solid State Ionics*, 1998, **110**, 103-110.
8. S. V. Bhide and A. V. Virkar, *Journal of The Electrochemical Society*, 1999, **146**, 2038-2044.
9. D. Pergolesi, E. Fabbri, A. D'Epifanio, E. Di Bartolomeo, A. Tebano, S. Sanna, S. Licoccia, G. Balestrino and E. Traversa, *Nature Materials*, 2010, **9**, 846-852.
10. N. Zakowsky, S. Williamson and J. Irvine, *Solid State Ionics*, 2005, **176**, 3019-3026.
11. L. Bi, S. Zhang, S. Fang, Z. Tao, R. Peng and W. Liu, *Electrochemistry Communications*, 2008, **10**, 1598-1601.
12. W. Sun, S. Fang, L. Yan and W. Liu, *Journal of The Electrochemical Society*, 2011, **158**, B1432.
13. C. Zuo, S. Zha, M. Liu, M. Hatano and M. Uchiyama, *Advanced Materials*, 2006, **18**, 3318-3320.
14. L. Bi, S. Zhang, S. Fang, L. Zhang, K. Xie, C. Xia and W. Liu, *Electrochemistry Communications*, 2008, **10**, 1005-1007.
15. Z. Gao, L. V. Mogni, E. C. Miller, J. G. Railsback and S. A. Barnett, *Energy Environ. Sci.*, 2016, **9**, 1602-1644.
16. N. Mahato, A. Banerjee, A. Gupta, S. Omar and K. Balani, *Progress in Materials Science*, 2015, **72**, 141-337.
17. C. Sun, R. Hui and J. Roller, *Journal of Solid State Electrochemistry*, 2010, **14**, 1125-1144.
18. K. Xie, R. Yan and X. Liu, *Electrochemistry Communications*, 2009, **11**, 1618-1622.
19. J. Hou, Z. Zhu, J. Qian and W. Liu, *Journal of Power Sources*, 2014, **264**, 67-75.
20. Z. Tao, L. Bi, L. Yan, W. Sun, Z. Zhu, R. Peng and W. Liu, *Electrochemistry Communications*, 2009, **11**, 688-690.
21. Z. Tao, L. Bi, Z. Zhu and W. Liu, *Journal of Power Sources*, 2009, **194**, 801-804.
22. Z. Zhu, J. Qian, Z. Wang, J. Dang and W. Liu, *Journal of Alloys and Compounds*, 2013, **581**, 832-835.
23. A. Evans, J. Martynczuk, D. Stender, C. W. Schneider, T. Lippert and M. Prestat, *Advanced Energy Materials*, 2015, **5**, 1400747.
24. Z. Zhu, Z. Tao, L. Bi and W. Liu, *Materials Research Bulletin*, 2010, **45**, 1771-1774.
25. Y. Ling, L. Zhao, X. Liu and B. Lin, *Fuel Cells*, 2015, **15**, 384-389.
26. A. Grimaud, F. Mauvy, J. Marc Bassat, S. Fourcade, M. Marrony and J. Claude Grenier, *Journal of Materials Chemistry*, 2012, **22**, 16017.
27. W. Sun, L. Yan, B. Lin, S. Zhang and W. Liu, *Journal of Power Sources*, 2010, **195**, 3155-3158.
28. W. Sun, Z. Shi, S. Fang, L. Yan, Z. Zhu and W. Liu, *International Journal of Hydrogen Energy*, 2010, **35**, 7925-7929.
29. F. He, T. Wu, R. Peng and C. Xia, *Journal of Power Sources*, 2009, **194**, 263-268.
30. C. Yang and Q. Xu, *Journal of Power Sources*, 2012, **212**, 186-191.
31. H. Ding and X. Xue, *International Journal of Hydrogen Energy*, 2010, **35**, 4311-4315.
32. B. H. Rainwater, M. Liu and M. Liu, *International Journal of Hydrogen Energy*, 2012, **37**, 18342-18348.
33. R. Chiba, H. Taguchi, T. Komatsu, H. Orui, K. Nozawa and H. Arai, *Solid State Ionics*, 2011, **197**, 42-48.
34. A. A. Taskin, A. N. Lavrov and Y. Ando, *Progress in Solid State Chemistry*, 2007, **35**, 481-490.
35. S. Sengodan, S. Choi, A. Jun, T. H. Shin, Y.-W. Ju, H. Y. Jeong, J. Shin, J. T. S. Irvine and G. Kim, *Nat Mater*, 2015, **14**, 205-209.
36. L. Bi, Z. Tao, W. Sun, S. Zhang, R. Peng and W. Liu, *Journal of Power Sources*, 2009, **191**, 428-432.
37. W. Sun, L. Yan, Z. Shi, Z. Zhu and W. Liu, *Journal of Power Sources*, 2010, **195**, 4727-4730.
38. C. J. Howard, G. R. Lumpkin, R. I. Smith and Z. Zhang, *Journal of Solid State Chemistry*, 2004, **177**, 2726-2732.
39. Y. Ling, J. Yu, B. lin, X. Zhang, L. Zhao and X. Liu, *Journal of Power Sources*, 2011, **196**, 2631-2634.
40. Q. Li, L.-P. Sun, L.-H. Huo, H. Zhao and J.-C. Grenier, *Journal of Power Sources*, 2011, **196**, 1712-1716.
41. W. Sun, Z. Zhu, Y. Jiang, Z. Shi, L. Yan and W. Liu, *International Journal of Hydrogen Energy*, 2011, **36**, 9956-9966.
42. Y. Ding, Y. chen, X. Lu and B. Lin, *International Journal of Hydrogen Energy*, 2012, **37**, 9830-9835.
43. Y. Chen, Q. Gu, D. Tian, Y. Ding, X. Lu, W. Yu, T. T. Isimjan and B. Lin, *International Journal of Hydrogen Energy*, 2014, **39**, 13665-13670.
44. Z. Gong, J. Hou, Z. Wang, J. Cao, J. Zhang and W. Liu, *Electrochimica Acta*, 2015, **178**, 60-64.